Intraocular scattering compensation in retinal imaging

Dimitrios Christaras[1,2,*], Harilaos Ginis[1,3], Alexandros Pennos[1] and Pablo Artal[1]

[1] *Laboratorio de óptica, Instituto Universitario de Investigación en óptica y nanofísica, Universidad de Murcia, Campus de Espinardo (Edificio 34), E-30100, Murcia, Spain*
[2] *UCL Institute of Ophthalmology, EC1V 9EL, London, UK*
[3] *Athens Eye Hospital 45, 166 75, Athens, Greece*
[*] *d.christaras@ucl.ac.uk*

Abstract: Intraocular scattering affects fundus imaging in a similar way that affects vision; it causes a decrease in contrast which depends on both the intrinsic scattering of the eye but also on the dynamic range of the image. Consequently, in cases where the absolute intensity in the fundus image is important, scattering can lead to a wrong estimation. In this paper, a setup capable of acquiring fundus images and estimating objectively intraocular scattering was built, and the acquired images were then used for scattering compensation in fundus imaging. The method consists of two parts: first, reconstruct the individual's wide-angle Point Spread Function (PSF) at a specific wavelength to be used within an enhancement algorithm on an acquired fundus image to compensate for scattering. As a proof of concept, a single pass measurement with a scatter filter was carried out first and the complete algorithm of the PSF reconstruction and the scattering compensation was applied. The advantage of the single pass test is that one can compare the reconstructed image with the original one and see the validity, thus testing the efficiency of the method. Following the test, the algorithm was applied in actual fundus images in human eyes and the effect on the contrast of the image before and after the compensation was compared. The comparison showed that depending on the wavelength, contrast can be reduced by 8.6% under certain conditions.

OCIS codes: (290.2648) Stray light; (290.5820) Scattering measurements; (100.2980) Image enhancement; (110.3010) Image reconstruction techniques; (330.5370) Physiological optics; (170.4460) Ophthalmic optics and devices.

References and links

1. F. W. Campbell and . H. Gregory, "Effect of size of pupil on visual acuity," Nature **187**, 1121–1123 (1960).
2. G. Westheimer and J. Liang, "Influence of ocular light scatter on the eye's optical performance," Journal of the Optical Society of America. A, Optics, image science, and vision **12**, 1417–1424 (1995).
3. T. J. T. P. VanderBerg, L. Franssen, and J. E. Coppens, "Ocular Media Clarity and Straylight," Encyclopedia of Eye **3**, 173–183 (2010).
4. J. Liang, D. Williams, and D. B. Miller, "Supernormal vision and high-resolution retinal imaging through adaptive optics," Journal of the Optical Society of America A: Optics and Image Science, and Vision **14**, 2884–2892 (1997).
5. J. Rha, R. S. Jonnal, K. E. Thorn, J. Qu, Y. Zhang, and D. T. Miller, "Adaptive optics flood-illumination camera for high speed retinal imaging," Optics express **14**, 4552–4569 (2006).
6. E. J. Fernández, I. Iglesias, and P. Artal, "Closed-loop adaptive optics in the human eye," Optics Letters **26**, 746–748 (2001).
7. A. Roorda, F. Romero-Borja, W. J. Donnelly, H. Queener, T. J. Hebert, and M. C. W. Campbell, "Adaptive optics scanning laser ophthalmoscopy," Optics Express **10**, 405–412 (2002).
8. T. Y. Chui, H. Song, and S. a. Burns, "Adaptive-optics imaging of human cone photoreceptor distribution," Journal of the Optical Society of America. A, Optics, image science, and vision **25**, 3021–3029 (2008).
9. A. Dubra, Y. Sulai, J. L. Norris, R. F. Cooper, A. M. Dubis, D. R. Williams, and J. Carroll, "Noninvasive imaging of the human rod photoreceptor mosaic using a confocal adaptive optics scanning ophthalmoscope," Biomedical Optics Express **2**, 1864–1876 (2011).
10. R. J. Zawadzki, S. M. Jones, S. S. Olivier, M. Zhao, B. A. Bower, J. A. Izatt, S. Choi, S. Laut, and J. S. Werner, "Adaptive-optics optical coherence tomography for high-resolution and high-speed 3D retinal in vivo imaging," Optics express **13**, 8532–8546 (2005).
11. M. Pircher, R. J. Zawadzki, J. W. Evans, J. S. Werner, and C. K. Hitzenberger, "Simultaneous imaging of human cone mosaic with adaptive optics enhanced scanning laser ophthalmoscopy and high-speed transversal scanning optical

coherence tomography," Optics letters **33**, 22–24 (2008).
12. I. Iglesias and P. Artal, "High-resolution retinal images obtained by deconvolution from wave-front sensing," Optics Letters **25**, 1804–1806 (2000).
13. D. Catlin and C. Dainty, "High-resolution imaging of the human retina with a Fourier deconvolution technique," Journal of the Optical Society of America. A, Optics, image science, and vision **19**, 1515–1523 (2002).
14. F. Flamant, "Etude de la repartition de lumiere dans l'image retinienne d'une fente," Revue d'Optique **34**, 433–459 (1955).
15. F. W. Campbell and R. W. Gubisch, "Optical quality of the human eye," The Journal of physiology **186**, 558–578 (1966).
16. H. Ginis, G. M. Pérez, J. M. Bueno, and P. Artal, "The wide-angle point spread function of the human eye reconstructed by a new optical method," journal of vision **12**, 1–10 (2012).
17. J. J. Vos and T. J. T. P. VanderBerg, "Report on disability glare," CIE Collection on Colour and Vision **135** (1999).
18. H. S. Ginis, G. M. Perez, J. M. Bueno, A. Pennos, and P. Artal, "Wavelength dependence of the ocular straylight," Investigative ophthalmology & visual science **54**, 3702–8 (2013).
19. G. D. Boreman, *Modulation transfer function in optical and electro-optical systems,* 2001. ISBN 0819441430.
20. H. Ginis, O. Sahin, A. Pennos, and P. Artal, "Compact optical integration instrument to measure intraocular straylight," Biomedical Optics Express **5**, 3036 (2014).
21. G. C. De Wit, L. Franssen, J. E. Coppens and T. J. T. P. Van Den Berg, "Simulating the straylight effects of cataracts," Journal of Cataract and Refractive Surgery, **32**, 294âĂŞ-300 (2006).
22. J. van de Kraats and D. van Norren, "Directional and nondirectional spectral reflection from the human fovea," Journal of Biomedical Optics **13**, 024010 (2014).
23. F. C. Delori and K. P. Pflibsen, "Spectral reflectance of the human ocular fundus," Applied Optics **28**, 1061–1077 (1989).
24. T. T. J. M. Berendschot, P. J. DeLint, and D. van Norren, "Fundus reflectance–historical and present ideas," Progress in retinal and eye research **22**, 171–200 (2003).
25. D. Christaras, H. Ginis, and P. Artal, "Spatial properties of fundus reflectance and red - green relative spectral sensitivity," Journal of the Optical Society of America A **32**, 1723–1728 (2015).
26. P. E. Kilbride, K. R. Alexander, M. Fishman, and G. A. Fishman, "Macular pigment assessed by imaging fundus reflectometry," Vision Research **29**, 663–674 (1989).
27. F. C. Delori, D. G. Goger, B. R. Hammond, D. M. Snodderly, and S. A. Burns, "Macular pigment density measured by autofluorescence spectrometry : comparison with reflectometry and heterochromatic flicker photometry," Journal of the Optical Society of America A **18**, 1212–1230 (2001).
28. T. T. J. M. Berendschot and D. Van Norren, "Objective determination of the macular pigment optical density using fundus reflectance spectroscopy," Archives of Biochemistry and Biophysics **430**, 149–155 (2004).
29. T. T. J. M. Berendschot, "Imaging the Macular Pigment," Medical Retina pp. 51–68 (2010).
30. A. O'Brien, C. Leahy, and C. Dainty, "Imaging system to assess objectively the optical density of the macular pigment in vivo," Applied optics **52**, 6201–6212 (2013).

1. Introduction

When imaging the fundus, the optical media have an effect on the image quality. Diffraction at the pupil and aberrations dominate exclusively the central part of the PSF thus affecting higher frequencies. Visually, that is perceived as a decrease in acuity and in contrast sensitivity [1]. Scattering, on the other hand, affects both high and low frequencies and depends on the dynamic range of the image and it is visually perceived as a loss of contrast sensitivity with a strong dependance on the presence of glare sources [2, 3].

The effects of high and low order aberrations in fundus imaging have been successfully measured and corrected. The use of adaptive optics made it possible for a dynamic, high-speed correction of the eye's aberrations in any fundus imaging device, from the simple fundus camera [4–6], to the confocal scanning laser ophthalmoscope (cSLO) [7–9] or the optical coherence tomography (OCT) [10, 11]. Moreover, the idea of a deconvolution of the fundus image with the measured wavefront was also suggested as a method of enhancing image quality [12, 13]. Although aberrations have been extensively studied and efficiently corrected, less research has been done for the correction of scattering in fundus imaging.

In this article, we suggest a customized approach which allows the enhancement of a fundus image compensating the contrast lost associated with intraocular scattering. For this purpose a setup to acquire fundus images was built which could also objectively reconstruct the individual's wide-angle PSF which is dominated by scattering at large angles. The PSF reconstruction was

done based on the double pass principle [14, 15] using the optical integration method [16] and the contrast enhancement was achieved with appropriate filtering in the Fourier domain.

2. Methods

2.1. PSF retrieval

For the reconstruction of the PSF the method of optical integration was used [16], where a series of uniform discs of increasing radius was recorded with a camera after going twice through the optics of the eye. The intensity I at the center of the disc as recorded by the camera will be

$$I_c(\theta) = I_o \int_0^{\theta} 2\pi\phi PSF_{dp}(\phi)d\phi. \tag{1}$$

where I_o the initial intensity at the center, θ the radius of the disc in degrees of visual angle and PSF_{dp} the double-pass PSF of the eye. From equation (1) the PSF_{dp} will be

$$PSF_{dp}(\theta) = \frac{1}{2\pi\theta}\frac{dI_c'(\theta)}{d\theta}. \tag{2}$$

where $I_c' = I_c/I_o$. In practice, I_o can be approximated by the intensity at the center of the largest projected disc.

The double-pass PSF is the autocorrelation of the single-pass PSF, which for a symmetric PSF is identical to its selfconvolution. The single-pass PSF or the real PSF of the eye will be

$$PSF \equiv PSF_{sp} = \mathcal{F}^{-1}\left[\sqrt{\left|\mathcal{F}\left(PSF_{dp}\right)\right|}\right]. \tag{3}$$

where $\mathcal{F}$ and $\mathcal{F}^{-1}$ the forward and inverse Fourier transform respectively. Note here that the Fourier transform of a rotational symmetric function is a real function and therefore the Phase Transfer Function (PTF) is zero, allowing the above manipulation without any information loss.

A straightforward way to extract the PSF would be to measure the intensity at the center for a number of discs of different sizes and then use equation (2). This technique, however, has proven to be extremely sensitive to noise. A less noisy method is to assume a parametric form for the PSF and use it to fit the experimental data, which in this case is the intensities of the center of the disks. For this purpose we employed the CIE glare function [17]. The function reads

$$\begin{aligned} PSF_{CIE} = {} & \left[1 - \left(0.08\,(A/70)^4\right)\right] \\ & \left[\frac{9.2\times10^6}{[1+(\theta/0.0046)^2]^{1.5}} + \frac{1.5\times10^5}{[1+(\theta/0.045)^2]^{1.5}}\right] \\ & \left[1+1.6(A/70)^4\right]\left\{\left[\frac{400}{1+(\theta/0.1)^2} + 3\times10^{-8}\times\theta^2\right]\right. \\ & \left.+p\left[\frac{1300}{[1+(\theta/0.1)^2]^{1.5}} + \frac{0.8}{[1+(\theta/0.1)^2]^{0.5}}\right]\right\} \\ & + 2.5\times10^{-3}\times p[sr^{-1}]. \end{aligned} \tag{4}$$

where θ the angle in degrees, A the age and p a pigmentation coefficient, taking values 0, 0.5 and 1 for black, brown and light eyes respectively. The age was the free parameter to be determined by the fitting to the experimental data and the pigmentation p was set by simple observation of the subject's iris.

The procedure followed for the reconstruction of the single pass PSF from double pass intensity measurements was the following: Firstly, a set of glare functions were simulated from equation (4)

for age values between 10 and 120 and for the three different pigmentation levels 0, 0.5 and 1 and each function was associated with a scatter parameter S at $\theta = 3$ degrees. Then, a respective double pass glare function set was computed by taking the selfconvolution of the set of glare functions simulated above. Consequently, the intensities at the center of disks of radius θ were computed from the set of the simulated double pass glare functions using equation (1). Finally, the simulated intensity curve from the set of curves that best fitted the experimental data was found by minimizing the root-mean-square deviation (RMSD). The PSF of the eye was then the one corresponding to that intensity curve.

It needs to be noted that the glare function shown in equation (4) is based largely on psychophysical data where fundus diffusion is less relevant. In an optical system however, fundus diffusion can be dominant in the PSF, and its domain of contribution depends on the wavelength [18]. Therefore, to avoid the intrusion effect of fundus diffusion, the fit was limited to data over 2.5 degrees.

Once the one-dimensional PSF is reconstructed, the two-dimensional PSF is computed by simple rotating the former. The desired accuracy can be then achieved by choosing the appropriate number of spatial points.

2.2. Contrast Enhancement

The image can be restored by application of appropriate filtering in the Fourier domain.

$$Image_{orig} = \mathcal{F}^{-1}\left\{\mathcal{F}\left\{Image\right\}\frac{\mathcal{F}\left\{PSF_{diff}\right\}}{\mathcal{F}\left\{PSF_{scat}\right\}}\right\}. \tag{5}$$

or the special case of a square pupil the MTF is given by the relation

$$MTF_{diff} = 1 - \frac{f}{f_{cut}}. \tag{6}$$

where the cutoff frequency is defined as $f_{cut} = \frac{1}{\lambda(F|\#)}$ and $F|\#$ for the finite conjugate case is defined as

$$(F|\#)_{objectspace} = p/D \tag{7}$$

$$(F|\#)_{imagespace} = q/D. \tag{8}$$

where p and q the object and image distance respectively [19]. For the system used in this study D was taken to be 3.5mm and f_{cut} was found to be 111 cpd at 550nm.

The ratio of the diffraction limited over the scattering MTF denotes that the contrast increase at all frequencies is adjusted to the level of a scatter-free, diffraction limited system.

2.3. Experimental Setup and procedure

The experimental setup was built such that it was capable of capturing fundus images at various field sizes and for different wavelengths through an user-friendly custom graphical user interfaced, developed in MATLAB (MathWorks, Natick, MA, USA) for the control of the particular purpose system. Figure 1 shows a schematic representation of the instrument. It is designed to use the minimal amount of optical elements, minimizing thus the intrinsic scattering of the system and in its geometry was such that it minimizes the spurious light reflections from the instrument itself and the eye to be measured. A xenon lamp illuminates a wavelength filter, mounted on a filter wheel, followed by a diffusing fiber (LLG0338; Thorlabs, Newton, NJ, USA), a collimating lens (L5) and a motorized iris diaphragm (8MID10-40; Standa, Vilnius, Lithuania) which is used to create uniform disks. The light is then guided through the optics of the system and focused on the subject's retina. The light reflected from the ocular fundus (depicted in the figure in light blue)

after passing through the optics of the system is reflected through a half mirror and collected by an electron multiplying charge-coupled device camera (EMCCD, Luca; Andor, Belfast, UK). The camera was mounted on a translating stage and was able to move axially, in order to compensate for the subject's defocus and any chromatic aberrations. The camera was calibrated using a photometer (LS-100; Konica Minolta, Tokyo Japan) and a LCD monitor (Phillips, Amsterdam, Netherlands). A mechanical shutter (SH05 Optical Beam Shutter; Thorlabs, Newton, NJ, USA), controlled by a micro-controller (Arduino UNO, Arduino.cc, Italy), was synchronized with the EMCCD so that the duration of the illumination would be the same with the duration of the image capture to avoid unnecessary exposure of the eye to light.

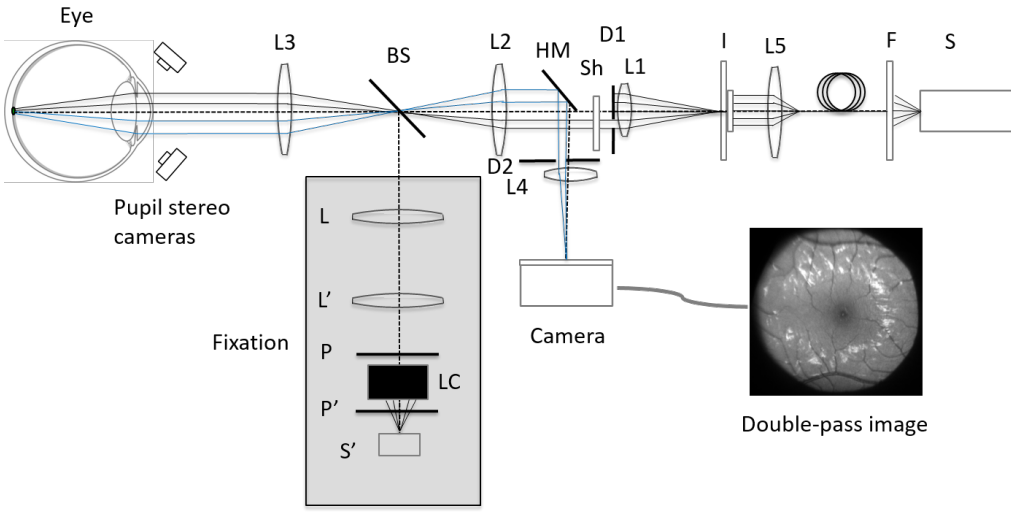

Fig. 1: Experimental setup. S, xenon lamp, F, wavelength filter, I, motorized Iris with diffuser, D1 and D2 rectangular diaphragms conjugate to the pupil, Sh, mechanical shutter, HM, half mirror and BS, beam splitter. In the light gray box the fixation subsystem with LC the LCoS and P, P' linear polarizers.

In order to be able to measure without the need of pupil dilation, the illumination duration was limited well below 0.3 seconds needed for pupil contraction. Indicatively, a measurement at 550nm lasted for less than 15 msec.

Two rectangular apertures, D1 and D2, 2 by 5 millimeters each, conjugates to the pupil plane were used. The aperture used for the illumination was conjugate to the upper part of the pupil whereas the one used for the imaging was conjugate to the lower part of the pupil, eliminating thus any back-scattered light from the lens or the cornea. The separation between the two apertures was 2mm so that no light is eliminated from an average dark adapted pupil.The above value was determined by taking into account the size of the maximum projected field and the physical and optical parameters of an average eye. The choice of rectangular apertures instead of the traditional circular ones permitted higher amount of light reaching the fundus with the same lateral separation.

This illumination/recording aperture setup requires a precise alignment of the eye, down to less than a millimeter because even a slight longitudinal shift can cause a contamination to the image from lens back-reflections. This was accomplished with a stereo sub-system consisting of two cameras and IR LEDs to illuminate the eye similar to that described in [20]. The micro-controller was used to turn off the IR illumination used by the two cameras stereoscopic system during the fundus measurement in order to avoid contaminating the measurement.

For the determination of the center of the recorded disk, in order to reduce errors due to thermal noise and involuntary eye movements, instead of taking a single point as the intensity at the center of each projected disk, the mean value of a central square patch of an area of 9x9 pixels, or roughly 16x16 minutes of arc was used.

As a first step, and as validation of the method before testing the eye, a projector (Optoma PK201 pico projector with a native resolution of 854×480) was used to project and capture images with and without the effect of scattering introduced by a scatter filter (Pro Mist; The Tiffen Company, NY), located at the pupil plane. First, the wide angle PSF of the filter was reconstructed according to the method of optical integration and then images of specific patterns with and without the filter were projected and captured by the camera. The reconstructed PSF was then used to reconstruct the image from the filtered image. Finally, the contrasts of the reconstructed image and the original image were compared, to validate the method.

After this test on the validity of the method, it was applied on eyes to retrieve the wide-angle PSF and then correct fundus images for the effect of scattering.

The subject fixated at about 8 degrees nasally (therefore the field is projected between the fovea and the optic disk), where the fundus exhibits higher uniformity with less absorbing structures such as veins or pigments, and it was then instructed to fixate at various positions around that position and a 7 degrees radius disk was projected on the retina and its image was then recorded. This was done in order to find a position where a central patch of about 2 degrees diameter was vein-free. The exposure time for the capture was adjusted in order to avoid pixel saturation and to assure that the recorded pixel values lie within the linear region of the camera response but high enough for a higher signal to noise ratio.

Once the vain-free area of the retina is located, the axial position of the camera is changed and more 7 degrees disks fundus images are taken in order to get the best focus of the retina on the camera, compensating this way any defocus caused by the subject's refractive errors and chromatic defocus. Since the motorized iris I (see figure 1) does not move in the same manner with the camera, this could cause a defocus in the illumination path, making the limits of the disks being out of focus, however, this does not affect the measurement.

During the previous two steps, a minimum number of 10 fundus images had to been taken. The procedure also assured the adaptation of the photoreceptors before starting the measurements. This was also tested in some preliminary tests where a number of disks of the same radius was projected on the retina over a period of 10 minutes and the intensity of a small patch of the recorded image was calculated. The test showed that after the first 5 images the photoreceptors were indeed adapted.

Consequently, after all parameters were set, a sequence of 21 discs was projected on the retina, varying from 0.4 to 6 degrees radius, and the images were captured by the camera. The procedure was repeated for all wavelengths, with the position of the camera changing to compensate the chromatic defocus.

It is important to note here that mainly due to dust particles the system also introduces some scattering that needs to be taken into account in the measurements. Therefore, in order to have an correct estimate for intraocular scattering, one needs to subtract the scattering of the system from each measurement. For the measurement of intraocular scattering of the system an artificial eye consisting of a 20mm plano-convex lens and a 99% reflective flat spectrum background was used, and the scattering was calculated using the same method as in real subjects.

2.4. Subjects

Six subjects, all Caucasians, with normal vision with no known pathology, between 24 and 35 years old participated in the study. Informed consent was obtained from the subjects after they were fully informed about the nature of the measurements. All subjects were measured at at least two wavelengths, with two subjects at three wavelengths and one subject at four wavelengths.

3. Results

3.1. Single pass Experiment

The optical integration algorithm was applied for the reconstruction of the profile of the PSF of a scatter filter (Pro Mist 1; The Tiffen Company, NY), where the glare function was used from equation (4) to simulate the PSF. Similar filters have been previously used to simulate the effect of cataracts [21]. The reconstructed profile of the filter's PSF is shown in figure 2.

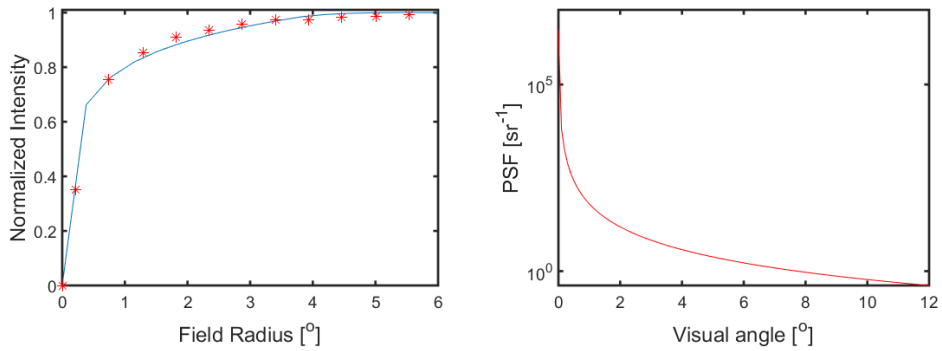

Fig. 2: Intensities at the center for different disk radii (left) and PSF profile (right) for scatter filter Pro Mist 1.

The 2D diffraction limited MTF was created according to equation (6). The original image was then reconstructed according to the image enhancement algorithm. The method was applied on an image showing a black "E" on white background, which was selected to show the visual aspect of scattering and how is a simple visual test affected by scattering. The results are shown below, where figure 3(a) shows the original image, figure 3(b) the image after scattering is applied and figure 3(c) the reconstructed image. In the letter images shown in figure 3(a) and figure 3(b), the

(a) (b) (c)

Fig. 3: (a) Original image. (b) Captured image through Pro Mist 1. (c) Reconstructed image

filter lowers the contrast of the image and smoothen the edges of the object. The reconstructed image using the contrast enhancement method is shown in figure 3(c). In order to make easier the quantitative comparison of the original and reconstructed image the profile plots for the three images is shown in figure 4, where the actual pixel values for the images are shown for a vertical profile.

3.2. Double pass image acquisition and simultaneous PSF retrieval

The procedure was done for six subjects. As an example, the intensities and the corresponding fittings for a subject D.C. for four different wavelengths are shown in figure 5.

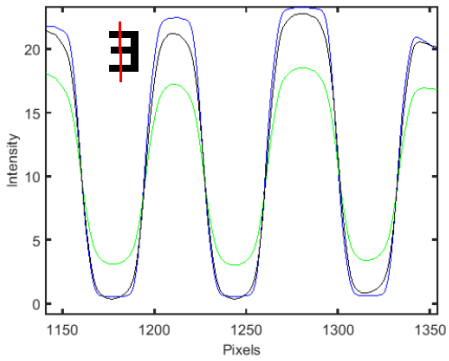

Fig. 4: Vertical profile of the original image (blue), the reconstructed (black) and the captured image with the effect of the filter (green), for letter E from the above figure.

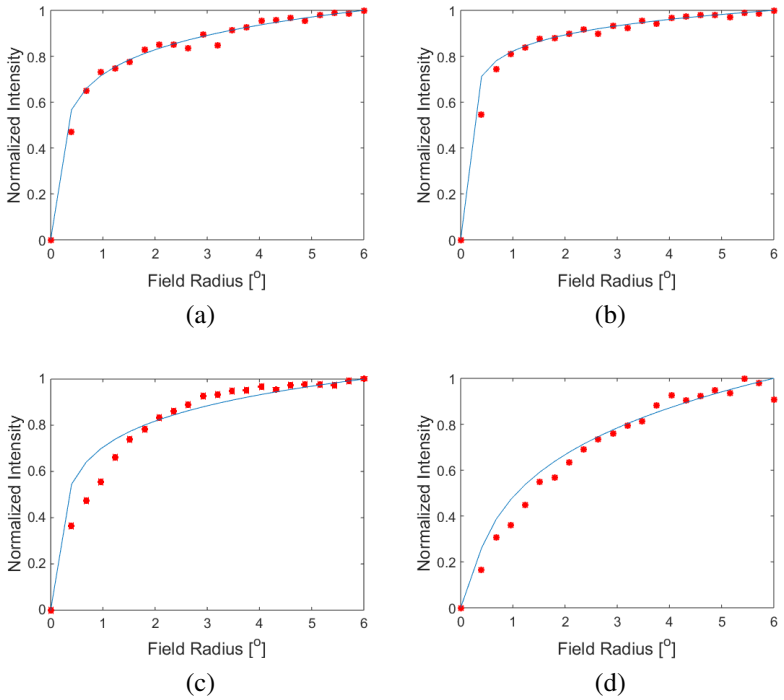

Fig. 5: Normalized intensity at the center of the projected disc with respect to disk radius in degrees at 450nm (a), 550nm (b), 632nm (c) and 800nm (d).

As mentioned in the Methods section, the function used for the data fit was based on psychophysical data and therefore it does not account for fundus diffusion effects, limiting the fit solely to data over 2.5 degrees. At shorter wavelengths, however, where diffusion at the fundus is minimal, the glare function is suitable to describe data even at narrow angles.

The reconstructed PSFs for all 4 wavelengths corresponding to the intensities shown in figures 5(a)-(d) are shown in figure 6.

In table 1 the logarithm of the scatter parameter S at 3 degrees is shown for all six subjects for the available wavelengths. Scattering is consistently lower at 550nm and higher for both 450nm

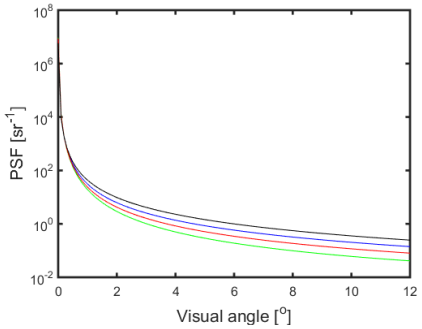

Fig. 6: PSF for subject D.C. at 450nm (blue), 550nm (green), 632nm (red) and 800nm (black).

and 632 and 800nm. More specifically, the mean value for the available subjects for 450nm was 1.26 (N=6, SD=0.08), for 550 was 1.06 (N=6, SD=0.13,21) and for 632 nm 1.15 (N=3, SD=0.10).

Table 1: Logarithm of the scatter parameter S at 3 degree for six subjects for the available wavelengths

	Log(S)			
Subject	**450nm**	**550nm**	**632nm**	**800nm**
B.L.	1.29	1.01	-	-
M.S.	1.21	0.98	-	-
A.P.	1.31	1.15	1.24	-
D.C.	1.35	0.96	1.15	1.91
J.M.	1.20	0.96	1.05	-
L.H.	1.15	1.05	-	-

3.3. Scattering compensation

The effect of scattering on a fundus image depends on the intrinsic scattering of the optical media and the initial contrast of the image. Generally, scattering reduces the contrast of the image by making bright features less bright and dark features less dark. For fundus images, the effect is higher at medium and short wavelengths where the contrast of the image is high due to absorbers like the macular pigment, the hemoglobin and the melanin. At longer wavelengths on the other hand, the lack of absorbing structures at those wavelengths, means that a fundus image would have low contrast and therefore, although the eye scatters more light, the effect on the image would not be as significant.

In order to give a more realistic idea of the effect of scattering in fundus imaging, the Weber contrast was calculated for a selected retinal feature before and after scattering compensation at 450nm and at 550nm for four subjects. Two examples are shown in figure 7 with the selected feature enclosed in a red square. The Weber contrast for fundus images at two different wavelengths before and after compensation for the selected features is shown in table 2.

From table 2 it can be seen that when scattering is not corrected, the Weber contrast for the selected features is underestimated. The relative increase when scattering is corrected depends on the intrinsic scattering of the eye at that wavelength but also on the contrast of the selected feature. At 550nm, however, where scattering is lower (see table 1), although the contrast is higher, the effect of scattering is minor due to the low intrinsic scattering.

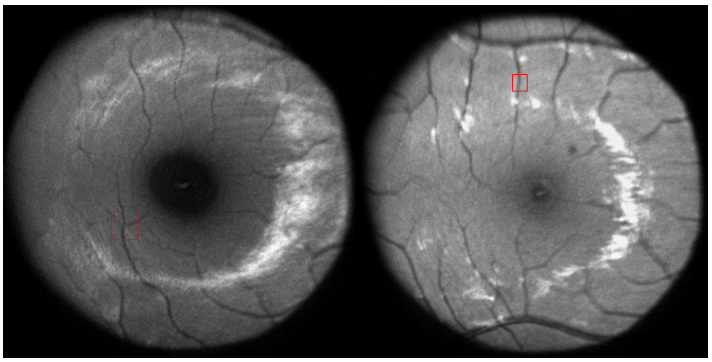

(a) (b)

Fig. 7: Fundus image taken at 450nm (a) and at 550nm (b). The feature used for the calculation of the Weber contrast is enclosed in the red rectangle.

Table 2: Weber contrast for selected features before and after scattering compensation.

		Weber Contrast		
Subject	**Wavelength [nm]**	**Before**	**After**	**Relative Increase [%]**
B.L	450	0.223	0.242	8.70
	550	0.460	0.472	2.60
D.C	450	0.441	0.459	4.13
	550	0.771	0.777	0.75
A.P.	450	0.502	0.516	2.82
	550	0.734	0.741	0.84
L.H.	450	0.468	0.484	3.50
	550	0.845	0.850	0.60

4. Discussion

Using the method of optical integration [16, 18] the wide angle PSF was reconstructed for various wavelengths and it was then used to compensate its effect in fundus imaging. This compensation had an effect on the contrast of the image with an increase of 8.7%. The amount of the increase depends on two factors: the amount of scattering the eye has at the particular wavelength but also the dynamical range of the image. The latter means that the effect of scattering will be greater, or better more noticeable, when the image has both high reflective and high absorbing areas, in the same way that visually, scattering is much more noticeable when driving at night, where the dynamic range is large due to the headlights, than when at day.

A first result, is the consistently lower amount of scattering at green, compared to blue and red, which is in line with a previous study [18]. For the longer wavelengths, however, there is an additional parameter that needs to be taken into account: melanin pigmentation. As shown in previous studies, fundus reflectance at longer wavelengths depends heavily on melanin pigmentation [22–25]. Low pigmentation individuals show a much higher fundus diffusion at longer wavelengths that significantly affect the PSF even for larger angles. In order to avoid such contribution from the fundus, for longer wavelengths the fitting domain was limited to over 3.5 degrees. For a single subject, scattering was measured also at 800nm. However, since the two main absorbers of the fundus, the melanin and the hemoglobin, are practically transparent in the

IR domain, fundus diffusion is significantly higher than at shorter wavelengths and therefore any contributions from the optics are masked by the increased fundus diffusion.

On a technical aspect of the method, there are two important points that one needs to take into account in order to correctly reconstruct the PSF: the sample density and the parity of the number of sampled points. In order to have an accurate reconstruction of the PSF, one would ideally need a very high sampling. This, however, is not always practical and it is limited by the computational power. Therefore, a clever choice of sampling is needed in order for the simulated PSF to be a good approximation of the continuous one, but within a reasonable time. The parity, on the other hand, becomes more important when the sampling is relatively low. This is due to the fact that the PSF, for very small angles, well below 0.1 degrees, increases dramatically, with its peak being two or more log units higher than the second point for a reasonable number of points. As expected, the profiles of the two PSFs are almost identical except for the very first points close to 0 degrees, where the odd sampled PSF is almost 2 log units higher. What, at a PSF level, might seem unimportant, it has an immense effect on the MTF. In case where the number of points is sufficiently large, the parity of the sampling becomes less important, but still the MTF is better approximated using an odd number of points.

The absolute contrast of a fundus image is not always of interest. In many cases algorithms to artificially increase the contrast of an image are used, especially when qualitative characterization of a fundal structure is the objective. There are, however, cases where the actual contrast of the fundus is of interest, with most important example that of macular pigment optical density (MPOD) measurements using the reflectometry method, where MPOD is calculated using the intensities of two fundus images, one at short and one at medium wavelength [26–30]. In this case, scattering would decrease contrast in the two images differently, leading to an underestimation of MPOD.

Finally, it needs to be underlined, that for a conventional fundus camera, which are not perfectly optimized to avoid lens back-scattered light, the contrast reduction due to scattering can be stronger and the above technique can only partially correct for scattering in system of this kind. On the other hand, in systems based on confocality such as the cSLO, scattering phenomena are not significant and it would not gain from a contrast enhancement technique like the above.

5. Conclusion

A method for the compensation of scattering in fundus imaging was developed, leading to a contrast enhancement of up to 8.7% depending on the conditions. The method consisted of two parts: The optical quantization of scattering of the individual for a particular wavelength and its consequent compensation in a fundus image taken at the above wavelength. This hybrid (optical-computational) approach can be of potential use when incorporated in instruments where quantitative fundus reflection data are required.

6. Funding

This research has been supported by the European Research Council Advanced Grant ERC-2013-AdG-339228 (SEECAT), the Spanish SEIDI, grant FIS2013-41237-R and the European Commission PITN-GA-2010-264605 (ITN OpAL).